

Carrier mobility and density of states in microcrystalline silicon film compositions, probed using time-of-flight photocurrent spectroscopy*

S. REYNOLDS*

Division of Electronic Engineering and Physics, University of Dundee, Nethergate, Dundee DD1 4HN, UK.

The technique of time-of-flight photocurrent spectroscopy, and its application in the study of carrier transport in microcrystalline silicon films over a range of material compositions, is described. Measurements reveal that the hole mobility is greatly increased in comparison to amorphous films, by up to a factor of 300 at room temperature, at a Raman crystalline volume fraction of 30% or more. Significant enhancements are evident at concentrations below 10%. A more modest increase in the electron mobility, by up to a factor of five, is found in highly crystalline films, while in low-crystallinity films the electron mobility appears to fall substantially *below* that measured in amorphous silicon. This is consistent with the poor blue response observed in the corresponding thick p-i-n solar cells. A comparison of results from time-of-flight and transient photocurrent techniques applied to films prepared at higher crystallinities reveals differences in the density of states distributions, which suggest that charge transport in these films may be anisotropic.

(Received November 5, 2008; accepted December 15, 2008)

Keywords: Microcrystalline silicon, Photoconductivity, Drift mobility, Computer simulation

1. Introduction

Microcrystalline silicon ($\mu\text{-Si:H}$) is an attractive thin-film semiconductor for large-area applications. Its increased optical absorption over amorphous silicon (a-Si:H) in the long wavelength region of the solar spectrum, coupled with a greater resistance to light-induced degradation, make it particularly suited as a bottom-cell active layer in tandem solar cells [1,2]. In addition, increased electron and hole mobilities have led to improvements [3] in thin-film transistor performance, to the point where CMOS structures are now feasible. These advances have been made largely through better understanding, control and optimisation of deposition processes, and in the case of solar cells, improvements in the optical design. The link between structure and electronic properties, although based on sound physical reasoning, remains largely empirical.

Fig. 1 is a cartoon depicting the wide range of film structures and compositions that may be obtained by changing appropriate deposition parameters, such as the proportion of silane in the process gas, $r = [\text{silane}] : [\text{silane} + \text{hydrogen}]$, with lower percentages of silane yielding more crystalline films [4]. In general, films are composed

of crystallites, voids and amorphous regions, and in the more crystalline material there is a tendency for small grains to aggregate into larger columnar structures aligned axially in the direction of film growth. Frequently, the Raman integrated intensity ratio I_{CRS} [4] is used to enable comparisons of crystalline content over a series of samples to be made. The degree of porosity and hydrogen content also varies with deposition conditions and with the choice of substrate [5].

There is currently no agreed universal model of carrier transport in $\mu\text{-Si:H}$. However there are two frameworks by which a number of the electronic properties observed over a range of compositions, temperatures and doping may be understood. One is in terms of a three-dimensional percolation of carriers [6,7] via more conducting (crystalline) regions embedded in less conducting regions (amorphous silicon and voids). This model has been shown to account for the conductivity transitions observed in doped $\mu\text{-Si:H}$ at around 30% crystallinity. The second is by trap-controlled conduction, either by hopping (typically when the Fermi energy is shallow, as in doped material) or by multiple-trapping [8], where the progress of carriers in extended states is mediated by trapping in

* Paper presented at the International School on Condensed Matter Physics, Varna, Bulgaria, September 2008

and emission from localized states. The latter model [9], is essentially an extension of that used to describe transport in a-Si:H [10] at moderate temperatures. In the case of μ -c-Si:H, there are crystalline grains and columns, amorphous regions, cracks and voids, separated by complex interfaces,

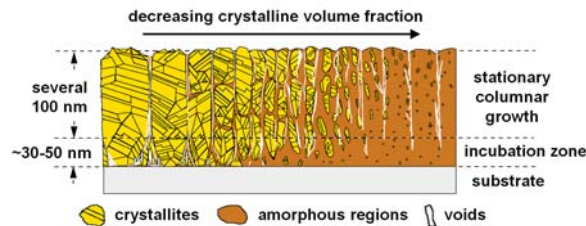


Fig. 1. Schematic representation of a silicon thin film, after Vetterl et al [2].but the general assumption is that band-like extended states, disorder-related tail states, and dangling-bond defects which may be passivated by hydrogen, largely define the electronic landscape and control charge transport [9].

In this paper, we report on the application of time-of-flight (TOF) spectroscopy to the study of carrier transport in microcrystalline silicon films prepared over a range of compositions. TOF measures the decay in current following a flash of strongly-absorbed light incident on one or the other blocking contact, on either sides of the film, between which a uniform electric field is maintained. In our experiments we make use of p-i-n solar cell structures, equipped with transparent top and bottom contacts. This allows us to investigate transport of electrons or holes, by directing the laser pulse from the p or the n side respectively. Extraction of carriers results in a fall in the photocurrent, which enables the transit time to be identified and the mobility calculated. The decays are analyzed in detail, to obtain the density of localized states (DOS) distribution vs. energy.

2. Experimental

2.1. TOF measurement

A typical experimental set-up for TOF is shown in Fig. 2. When the laser is fired, normally under computer control, the bias supply pulse generator is immediately triggered from a fast photodiode. Typically we use a green laser dye, such as Coumarin 500, which in μ -c-Si:H results in an absorption depth of some 160 nm. A pulsed voltage supply is used to maintain a uniform field over the experimental timescale, which must therefore be less than the dielectric relaxation time. For μ -c-Si:H, which has a relatively high conductivity, this may be 1 μ s or less at 300K. To enable the large displacement current due to the leading edge of the field pulse to decay, the laser pulse may be delayed for a few microseconds using a drum of optical fibre. It then hits the sample, and simultaneously triggers the

oscilloscope used to record the current transient to acquire data ($t = 0$). The current transient is converted to a voltage using a resistance; often 50 ohms is used at the shortest times to provide a match to the coaxial cable and to keep RC time-constants low (< 10 ns). At longer times, larger resistors or a current preamplifier (with DC offset control to null out the dark current) may be used. Some pre-trigger points are normally included and may be used to define the current baseline, which is subsequently subtracted from the data. Alternatively, the baseline may be measured separately, using a shutter to prevent light from reaching the sample.

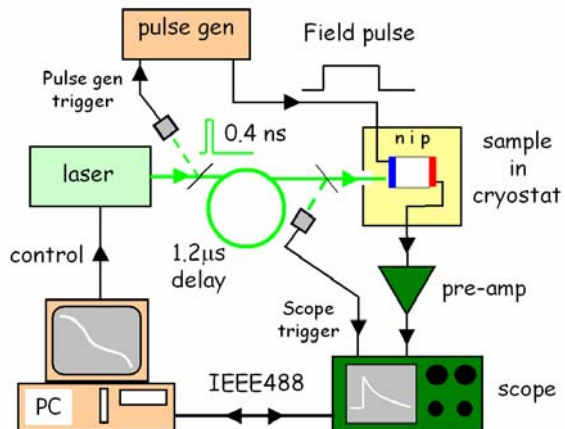


Fig. 2. Time of flight measurement system (shown configured for hole TOF).

In order not to distort the applied electric field, the total photocharge should not exceed the CV product, and the pulse intensity may be adjusted accordingly using neutral density filters. Repetitive averaging is used to improve the signal to noise ratio, with a pulse repetition rate sufficiently slow to allow the sample to approach thermal equilibrium between shots. Data are then transferred to a PC for baseline subtraction and further processing. Representative curves are shown in Fig. 3(a). For DOS analysis, a single current-time curve spanning several decades of time may be compiled from a mosaic of curves obtained on different timescales, as shown in Fig. 3(b). For a given sample, a series of experiments parametric in electric field and temperature is usually performed.

2.2 Data analysis

A fundamental consequence of multiple trapping is that the arrival of carriers at the collecting contact is spread out in time, as illustrated in Figs. 3(a), 3(b), as a result of the exponential relationship between trap depth and emission time. For shallow band tails, or at higher temperatures, this dispersion may both delay and obscure the downturn of the current-time graph at the transit time. Usually however, this may be identified on a log-log plot. The 50%

charge collection time may also be used, most effectively where the dispersion is large. It should be noted that as a consequence of dispersion, meaningful comparisons between the drift mobility measured by TOF for a range of samples may only be made when specified at the same ratio of thickness to electric field [11].

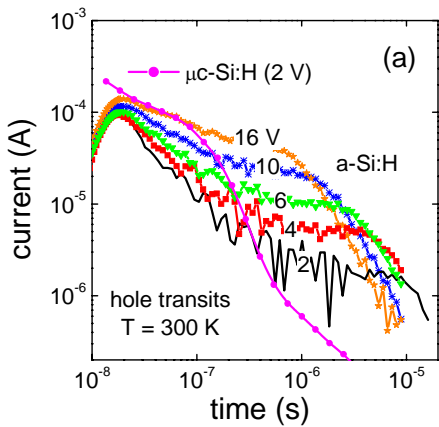


Fig. 3(a). Time of flight data parametric in bias voltage for an a-Si:H sample at 300 K. A μ c-Si:H curve is shown for comparison.

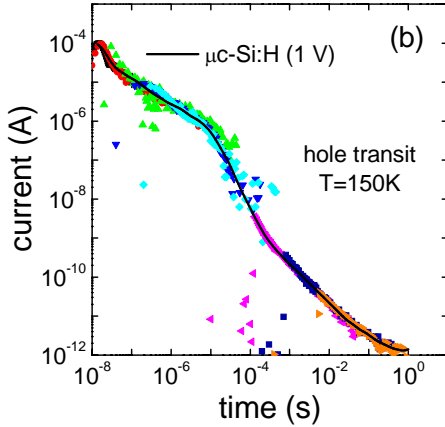


Fig. 3(b). TOF Data obtained from μ c-Si:H at 150 K, over eight orders of magnitude of time.

The analysis of photocurrent decay data to obtain the DOS may be carried out in a number of ways. If exponential bandtails whose characteristic energy is greater than kT are assumed to exist, then the current decay may be cast in terms of two power laws [10]: $I(t) \propto t^{-(1-\alpha)}$ in the pre-transit region and $I(t) \propto t^{-(1+\alpha)}$ in the post-transit region. $\alpha = E_0/kT$ is the dispersion parameter, where E_0 is the characteristic slope of the band tail of the majority carrier, k is Boltzmann's constant and T the experimental temperature. The current-time data at several temperatures may be force-fitted to the full pre-transit expression, and values for the band-tail slope and attempt to escape frequency extracted [11]. At least for

silicon thin films, the post-transit region is strongly affected by the presence of deeper states [12] and is seldom compatible with a single exponential distribution. More recently, 'spectroscopic' methods of analysis, *i.e.* those that do not assume a particular DOS, have been developed. These are based on Fourier [13] or Laplace [14] transformations of time-domain data and may be applied to the entire data range. These enable both band tails and deeper states to be probed. The DOS analysis carried out in this paper is based on the Fourier method.

2.3 Sample preparation

TOF p-i-n samples were prepared on 10 x 10 cm glass substrates using a cluster-tool system. Firstly, RF magnetron sputtered ZnO:Al was deposited onto a pattern of Al grid lines. A brief dip in dilute hydrochloric acid removed any protruding features from the TCO. A crystalline μ c-Si p-layer of thickness 30 nm was then grown, followed by a nominally 4 μ m thick i-layer, under high-pressure-high-power conditions of 2.1 mbar and 20 W [15], at a rate of typically 5 $\text{Å}/\text{s}$. The substrate temperature was approximately 200 °C. The process gas ratio r was used to control i-layer crystallinity. The junction was completed by deposition of a standard RFCVD (27 MHz) n-type a-Si:H layer 30 nm thick, and a back contact of patterned 2 mm diameter dots of sputtered ZnO:Al. Note that the i-layer thickness is greater than for a typical solar cell – this reduces the capacitance and lengthens transit times for a given applied voltage, which assists the system resolution at short times. Some samples were also prepared with 1 x 1 cm Ag back contacts, to facilitate standard solar cell characterization as required.

3. Results and discussion

3.1. Carrier mobilities

Electron and hole transits at 150 K for a highly-crystalline sample over a range of applied voltages are shown in Figs. 4(a), 4(b). The shapes of both sets of curves are consistent with dispersive transport [10], with the pre-transit current (after the initial system response) decaying roughly as a power-law. Arrhenius plots of the electron and hole mobilities presented in Fig. 5 reveal that carrier transport is thermally activated, in a similar way to a-Si:H. The data are generally in line with results reported previously [16–20], particularly regarding the large increase in hole mobility, of a factor of the order of 200 in μ c-Si:H ($I_{CRS} = 0.35, 0.6$) in comparison with a-Si:H. However, an enhancement in the hole mobility by a factor of 5, at a similar L/E ratio, is clearly seen at $I_{CRS} = 0.1$. Similar, but smaller, effects occur in polymorphous silicon [21] and a-Si:H prepared by the expanding thermal plasma (ETP) technique [22]. It has been suggested that the nanocrystalline inclusions found in polymorphous silicon result in improved medium-range ordering and thereby in a higher hole mobility. An alternative view would be that a higher mobility hole percolation path is somehow

established as the crystallinity increases, although a crystalline content of 10% is below the accepted range for 3-d percolation thresholds [6,7]. However, computer simulations in which an anisotropic (fibrous or filamentary) distribution is adopted [23], in closer agreement with the observed growth morphology shown in Fig. 1, suggest that transport in the direction of growth may in fact be dominated by crystalline material, even at such low concentrations.

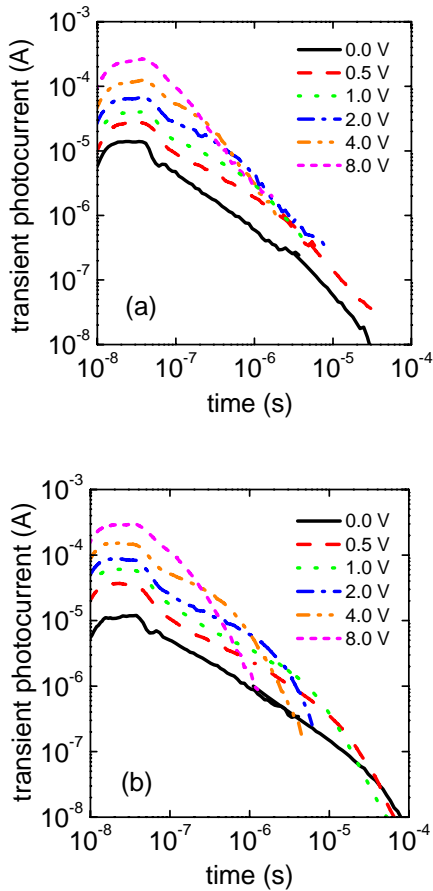


Fig. 4. (a) Electron and (b) hole transits for highly microcrystalline silicon ($4.3 \mu\text{m}$) measured at 150 K, parametric in bias voltage.

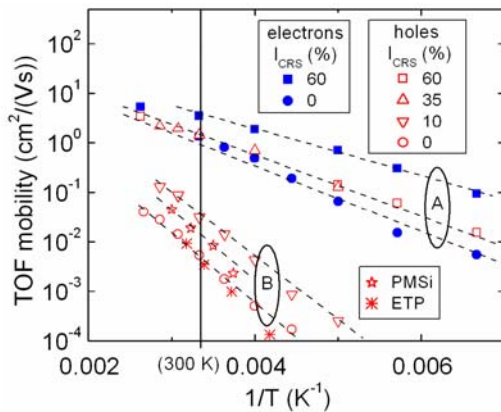


Fig. 5. Arrhenius plots of electron and hole mobility. L/E ratios are approximately 2×10^7 and $1 \times 10^8 \text{ cm}^2/\text{V}$ respectively for groups A and B. PMSi and ETP are hole mobility data for polymorphous and ETP silicon samples, taken from references 21 and 22, respectively.

We have also examined a series of samples prepared with very low crystallinity ($I_{CRS} < 10\%$). In our reactor, this corresponds to a process gas ratio r of 6 to 7%. This material is extremely sensitive to growth conditions, such that during the course of a single deposition, significant variations in crystallinity occur over the substrate area. Raman spectroscopy shows that for our system, the least crystalline material is found at the periphery of the substrate, and it becomes significantly more crystalline on moving towards the centre. The variation may range from nominally amorphous ($I_{CRS} = 0$) to about 10% crystalline ($I_{CRS} = 0.1$). A good correlation is found between I_{CRS} and the resulting solar cell open-circuit voltage V_{OC} . We have examined several such samples using TOF, and the hole mobility at just a few percent Raman crystallinity is significantly greater than in fully amorphous films prepared at high silane concentrations ($r > 10\%$), by a factor of 2 to 5. This suggests that there are similarities between this material and polymorphous silicon.

More recently, we have carried out *electron* TOF on these low-crystallinity samples. A careful examination reveals that electron mobilities are in fact significantly *reduced*, by as much as a factor of 10, when compared to a-Si:H. We have reported more fully on these findings elsewhere [24]. Such a reduction would be expected to have a significant adverse effect on solar cell performance, particularly for the thick cells used in this TOF work. In support, Fig. 6 shows the blue response vs. V_{OC} for several thick (4 μm) low-crystallinity samples, illuminated from the p-side. Electrons thus generated must drift the entire width of the i-layer to be collected. A pronounced minimum in the blue J_{SC} occurs, which mirrors the indicated variation in the electron mobility. This is exactly what is expected if there is an increased recombination loss of electrons. As may be

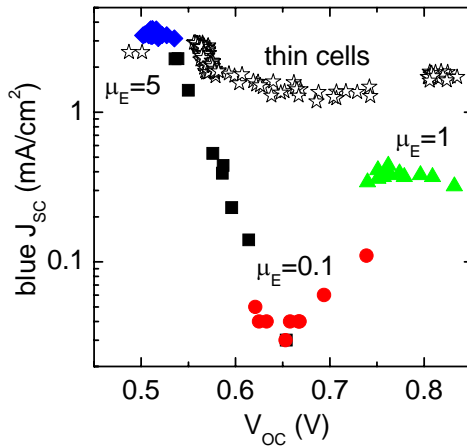


Fig. 6. Blue light short-circuit current density vs. open-circuit voltage (AM1.5) for several solar cells prepared with r between 5.5 and 10%. Note the logarithmic vertical axis. The open star symbol indicates data from thinner cells.

anticipated, a far less dramatic effect is seen in thin solar cells ($< 1 \mu\text{m}$) prepared under similar conditions. This also suggests that bulk, rather than interface, properties control solar cell performance in this case, as the interface should be independent of the i-layer thickness on a micron scale.

3.2 TOF Density of States parameters

Fig. 7 shows the DOS obtained by applying the Fourier transform analysis developed by Main *et al* [13]. The samples investigated here were prepared with $I_{CRS} = 60\%$. Separately, for electron and hole currents, the attempt-to-escape frequency v was adjusted to give the greatest degree of overlap in energy between the steeper DOS sections at different temperatures. The results imply a roughly exponential conduction band tail of about 22 meV, levelling into a fairly flat distribution of deep defects, and $v = 10^{12} \text{ s}^{-1}$. In contrast, the valence band states show a gradual fall near the band edge, followed by a steep fall at about 0.13 eV above E_V . Optimal alignment is obtained in this region assuming $v = 6 \times 10^9 \text{ s}^{-1}$. A similar steeply-falling valence-band DOS profile has been proposed by Ram *et al* [25], based on the intensity dependence of the steady-state photoconductivity.

The seemingly much larger defect density in this half of the gap should not necessarily be interpreted as such, as there is no clear temperature-dependent feature to be used for calibration. As the long-time post-transit currents for electrons and holes are of a similar magnitude, with a predominantly t^l slope, a more plausible estimate would be that the deep defect density is roughly uniform [12].

Fig. 8(a) shows computer simulations [26] of

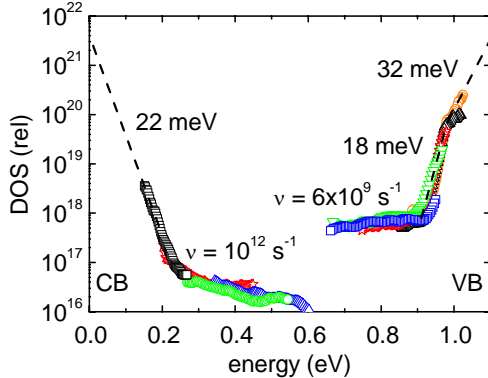


Fig. 7. Density of states plot obtained from TOF data using the Fourier transform method. Band-edge DOS fixed at $4 \times 10^{21} \text{ cm}^{-3} \text{ eV}^{-1}$.

TOF decays for a range of exponential band tail energies. No deep defects are included, and thus power law forms are expected [10]. By assuming a band mobility ($20 \text{ cm}^2/(\text{Vs})$), these may be translated into drift mobilities as shown in Fig 8(b). The experimental a-Si:H electron and hole and μ -c-Si:H electron mobilities map onto the $v = 10^{12} \text{ s}^{-1}$ curve, whereas the μ -c-Si:H hole mobility fits better to $v = 6 \times 10^9 \text{ s}^{-1}$. This supports the values of v deduced from the above DOS calculations. However, band offsets between amorphous and microcrystalline regions [9,27] could also give rise to peculiar features in the ‘apparent’ DOS.

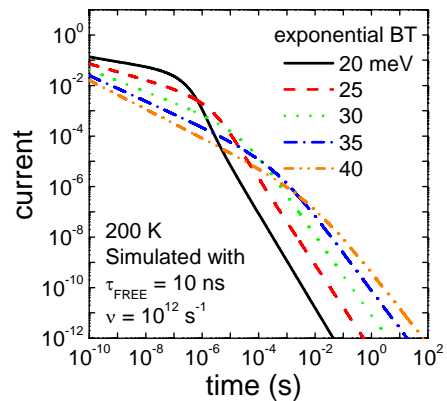


Fig. 8. (a) TOF current-time simulations with different bandtail slopes.

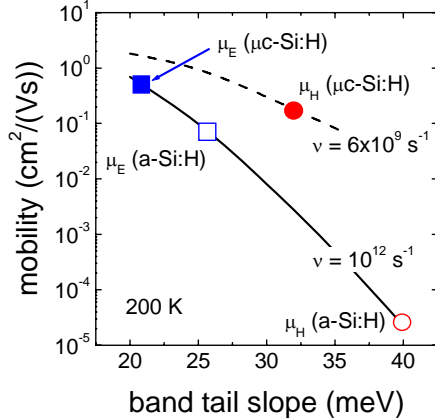


Fig. 8. (b) Mobilities calculated from transit times, assuming a free carrier mobility of $20 \text{ cm}^2/(\text{Vs})$, attempt-to-escape frequencies of 10^{12} and $6 \times 10^9 \text{ s}^{-1}$. Experimental values are denoted by symbols.

3.3 Comparison of the TOF and coplanar transient photoconductivity

Coplanar transient photoconductivity (TPC) may also be utilised in the study of microcrystalline silicon, as we

have previously reported [28,29]. While TPC and TOF are essentially similar, some important differences exist. In TPC, nett carrier transport occurs parallel to the film, and as the contacts are ohmic, carriers circulate around the external circuit until they undergo recombination in the film. In intrinsic material, TPC is sensitive primarily to the properties of the more mobile carrier. While it is not possible to measure the carrier mobility, multiple-trapping between localised and extended states enables the DOS to be extracted from the photocurrent decay, as per section 3.2.

Fig. 9 shows a collection of DOS plots, obtained for $\mu\text{-Si:H}$ and a-Si:H films, using both TPC [28,29] and TOF. In each case, the curves are scaled to the same band-edge DOS assuming the band tails extend to the mobility edge. In TPC, the applied electric field These observations support the view that $\mu\text{-Si:H}$ films are electrically as well as structurally anisotropic [29-31]. The sharper CB tail sampled by carriers travelling along the direction of growth (in TOF), rather than in the plane of the film (in TPC), is consistent with a greater degree of order, as might be found within the crystalline columns. However the CB tail is equally steep in good-quality a-Si:H , which is in conflict with this interpretation. High-quality a-Si:H appears to have a somewhat lower deep defect density than $\mu\text{-Si:H}$, measured using either

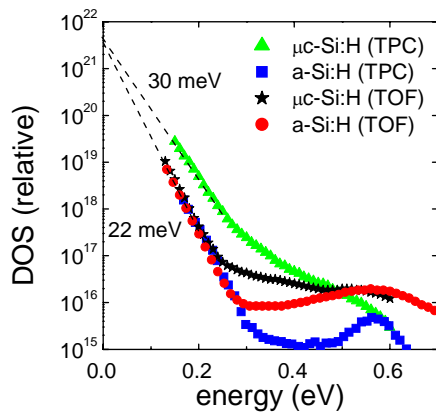


Fig. 9. DOS plots for $\mu\text{-Si:H}$ and a-Si:H obtained using TPC and TOF.

technique, suggesting that the amorphous tissue in mixed-phase $\mu\text{-Si:H}$ is of poorer quality than ‘homogeneous’ a-Si:H . This may be because passivating hydrogen is locked into grain boundaries and is therefore less readily available to terminate dangling bonds. For PECVD material, spin densities as high as 10^{17} cm^{-3} have been reported [32] for highly crystalline samples, falling below 10^{16} cm^{-3} for fully amorphous material. However, in the transition region there is evidence for a minimum in the spin density, which we have not observed in this work to date.

4. Conclusions

Time-of-flight photocurrent spectroscopy has been used successfully to study electron and hole transport in microcrystalline silicon. In comparison with amorphous silicon, the hole drift mobility measured by TOF is significantly enhanced by less than 10% of crystalline material in the film, and is some 200 times greater in highly-crystalline material. Three-dimensional percolation models cannot account for such strong effects at low crystallinity, and the similarity to polymorphous silicon suggests that enhanced medium-range order may play a part. It is also possible that thin fibres or filaments of higher hole mobility material extend through the film. The increase in the electron mobility in highly-crystalline material is small in comparison to that for holes, being no more than a factor of 5. Samples prepared with very low crystallinity, however, appear to show a significantly reduced electron mobility in comparison with amorphous silicon, which is supported by steady-state measurements of solar cell parameters such as blue response. It thus seems that low concentrations of crystalline material may simultaneously be beneficial to hole transport and detrimental to electron transport. Purely structural explanations, involving high-mobility crystalline pathways and low-mobility amorphous tissue, do not seem able to account for this, although they may of course be appropriate in more highly crystalline or doped films. Within a multiple-trapping framework, and assuming a homogeneous material, it is tempting to suggest that in the low-crystallinity regime ($I_{CRS} < 10\%$), the presence of ‘some crystallinity’ increases the ratio of transport states to shallow localised states for holes (VB), whilst doing the opposite for electrons (CB). We are currently developing these ideas quantitatively.

Applying TOF DOS spectroscopy to more highly-crystalline samples, an exponential CB tail of slope typically 22 meV is deduced, whereas the VB tail is rather broader at 32 meV. An adjustment of the transport parameters, such as a reduction in the attempt to escape frequency, is required for consistency with the high hole mobility and observed temperature-dependence of the photocurrent decays. A rapid fall in the DOS some 0.2 eV above the VB edge is predicted, however this may be connected with band offsets between amorphous and microcrystalline regions in the transport path rather than the DOS.

By comparing the TOF and TPC DOS plots for more highly-crystalline films, it is seen that the CB tail is somewhat broader when viewed using TPC, suggesting that the transport path for electrons parallel to the film is influenced by a greater structural disorder than that through the film. This is consistent with electron transport in TOF taking place predominantly along the crystalline columns, whereas in TPC the amorphous material between columns appears to exert a more significant influence. In general however, the deep defect density appears higher in $\mu\text{-Si:H}$ than in good quality a-Si:H , suggesting that an additional source of dangling bond defects, possibly at column boundaries, contributes to the total gap state density.

Acknowledgments

The author is most grateful to Reinhard Carius, Thorsten Dylla, Friedhelm Finger, Aad Gordijn, Markus Hülsbeck and Vlad Smirnov of IEF-5 Photovoltaik, Forschungszentrum Jülich, for their many important contributions to the data and ideas presented in this paper.

References

- [1] A. V. Shah, J. Meier, E. Vallat-Sauvain, N. Wyrtsch, U. Kroll, C. Droz, *Solar Energy Materials & Solar Cells* **78**, 469 (2003).
- [2] O. Vetterl, F. Finger, R. Carius, P. Hapke, L. Houben, O. Kluth, A. Lambertz, A. Mück, B. Rech, H. Wagner, *Solar Energy Materials & Solar Cells* **62**, 97 (2000).
- [3] C-H. Lee, A. Sazonov, A. Nathan, J. Robertson, *Appl. Phys. Lett.* **89**, 252101 (2006).
- [4] L. Houben, M. Luysberg, P. Hapke, R. Carius, F. Finger, H. Wagner, *Phil. Mag. A* **77**, 1447 (1998).
- [5] M. Tzolov, F. Finger, R. Carius, P. Hapke, *J. Appl. Phys.* **81**, 7376 (1997).
- [6] K. Shimakawa, *J. Non-Cryst. Solids* **266-269**, 223 (2000).
- [7] H. Overhof, M. Otte, in: *Proceedings of the Ninth International School on Condensed Matter Physics*, World Scientific, Singapore, 1997, p. 23.
- [8] J. M. Marshall, *Philos. Mag.* **36**, 959 (1977).
- [9] J. Kočka, A. Fejfar, H. Stuchlíková, J. Stuchlík, P. Fojtík, T. Mates, B. Rezek, V. Švrček, I. Pelant, *Solar Energy Materials & Solar Cells* **78**, 493 (2003).
- [10] T. Tiedje, in: J. D. Joannopoulos, G. Lucovsky (Eds.), *Hydrogenated Amorphous Silicon II*, Springer-Verlag, New York, pp261, 1984
- [11] Q. Wang, H. Antoniadis, E. A. Schiff, S. Guha, *Phys. Rev. B* **47**, 9435 (1993).
- [12] G. F. Seynhaeve, R. P. Barclay, G. J. Adriaenssens, J. M. Marshall, *Phys. Rev. B* **39**, 10196 (1989).
- [13] C. Main, *MRS Symp. Proc.* **467**, 167 (1997).
- [14] N. Ogawa, T. Nagase, H. Naito, *J. Non-Cryst. Sol.* **266**, 367 (2000).
- [15] Y. Mai, S. Klein, R. Carius, J. Wolff, A. Lambertz, F. Finger, X. Geng, *J. Appl. Phys.* **97**, 114913 (2005).
- [16] N. Wyrtsch, M. Goerlitzer, N. Beck, J. Meier, A. Shah, *Mat. Res Soc. Symp. Proc.* **420**, 801 (1996).
- [17] M. Serin, N. Harder, R. Carius, *J. Mat. Sci.: Mat. El.* **14**, 733 (2003).
- [18] A. Fejfar, N. Beck, H. Stuchlíková, N. Wyrtsch, P. Torres, J. Meier, A. Shah, J. Kočka, *J. Non-Cryst. Solids* **227-230**, 1006 (1998).
- [19] T. Dylla, F. Finger, E. A. Schiff, *Appl. Phys. Lett.* **87**, 032103 (2005).
- [20] T. Dylla, S. Reynolds, R. Carius, F. Finger, *J. Non-Cryst. Solids* **352**, 1888 (2006).
- [21] M. Brinza, G. J. Adriaenssens, P. R. I. Cabarrocas, *Thin Solid Films* **427**, 123 (2003).
- [22] M. Brinza, G. J. Adriaenssens, K. Iakoubovskii, A. Stesmans, W. M. M. Kessels, A. H. M. Smets, M. C. M. van de Sanden, *J. Non-Cryst. Solids* **299**, 420 (2002).
- [23] F. Liu, M. Zhu, Q. Wang, *Phys. Letts. A* **331**, 432 (2004).
- [24] S. Reynolds, R. Carius, F. Finger, V. Smirnov, *E-MRS Spring Meeting* (Strasbourg, May 26-30 2008), Symposium E. To appear in *Thin Solid Films* (2009).
- [25] S.K. Ram, S. Kumar, P. R. I. Cabarrocas, *J. Non-Cryst. Solids* **352**, 1172 (2006).
- [26] C. Main, R. Brüggemann, in *Electronic and Optoelectronic Materials for the 21st Century*, eds. J. M. Marshal, N. Kirov, A. Vavrek, World Scientific, Singapore, 1993, p279.
- [27] F. Finger, J. Müller, C. Malten, H. Wagner, *Philos. Mag. B* **77**, 805 (1998).
- [28] S. Reynolds, V. Smirnov, F. Finger, C. Main, R. Carius, *J. Optoelectron. Adv. Mater.* **7**, 91 (2005).
- [29] S. Reynolds, V. Smirnov, C. Main, R. Carius, F. Finger, *Mat. Res. Soc. Symp. Proc.* **715**, A21.2.1 (2002).
- [30] T. Unold, R. Brüggemann, J. P. Kleider, C. Longeaud, *J. Non-Cryst. Sol.* **266-269**, 325 (2000).
- [31] K. Hattori, Y. Musa, N. Murakami, N. Deguchi, H. Okamoto, *J. Appl. Phys.* **94**, 5071 (2003).
- [32] F. Finger, S. Klein, T. Dylla, A. L. Baia Neto, O. Vetterl, R. Carius, *MRS Symp. Proc.* **715**, A16.3.1 (2002).

*Corresponding author: s.z.reynolds@dundee.ac.uk